Demonstration of ultra-low NA rare-earth doped step index fiber for applications in high power fiber lasers

Deepak Jain,* Yongmin Jung, Pranabesh Barua, Shaiful Alam, and Jayanta K. Sahu

Optoelectronics Research Center, University of Southampton, Southampton SO17 1BJ, United Kingdom
**dj3g11@orc.soton.ac.uk*

Abstract: In this paper, we report the mode area scaling of a rare-earth doped step index fiber by using low numerical aperture. Numerical simulations show the possibility of achieving an effective area of ~700um^2 (including bend induced effective area reduction) at a bend diameter of 32cm from a 35μm core fiber with a numerical aperture of 0.038. An effective single mode operation is ensured following the criterion of the fundamental mode loss to be lower than 0.1dB/m while ensuring the higher order modes loss to be higher than 10dB/m at a wavelength of 1060nm. Our optimized modified chemical vapor deposition process in conjunction with solution doping process allows fabrication of an Yb-doped step index fiber having an ultra-low numerical aperture of ~0.038. Experimental results confirm a Gaussian output beam from a 35μm core fiber validating our simulation results. Fiber shows an excellent laser efficiency of ~81% and a M^2 less than 1.1.

OCIS codes: (060.2280) Fiber design and manufacturing; (140.3510) Fiber lasers.

References and links

1. C. Jauregui, J. Limpert, and A. Tunnermann, "High-power fiber lasers," [Invited], Nat. Photonics **7**, 861-867 (2013).
2. M. O'Connor, V. Gapontsev, V. Fomin, M. Abramov, and A. Ferin, "Power Scaling of SM Fiber Lasers toward 10kW," in *Conference on Lasers and Electro-Optics*(CLEO), Baltimore, MD, 2014, paper CThA3 (2009).
3. G. P. Agrawal, *Nonlinear Fiber Optics*, 4th ed. (Academic, 2007).
4. J. Limpert, A. Liem, M. Reich, T. Schreiber, S. Nolte, H. Zellmer, and A. Tunnermann, "Low-nonlinearity single-transverse-mode ytterbium-doped photonic crystal fiber amplifier," Opt. Exp. **12** (7), 1313-1319 (2004).
5. G. Gu, F. Kong, T. W. Hawkins, P. Foy, K. Wei, B. Samson, and L. Dong, "Impact of fiber outer boundaries on leaky mode losses in leakage channel fibers," Opt. Exp. **21** (20), 24039-24048 (2013).
6. R. A. Barankov, K. Wei, B. Samson, and S. Ramachandran, "Resonant bend loss in leakage channel fibers," Opt. Lett. **37** (15), 3147-3149 (2012).
7. E. M. Dianov, M. E. Likhachev, and S. Fevrier, "Solid-core photonic bandgap fibers for high-power fiber lasers," IEEE J. Sel. Top. Quant. Electron. **15** (1), 20-29 (2009).
8. G. Gu, F. Kong, T. Hawkins, J. Parsons, M. Jones, C. Dunn, M. T. Kalichevsky-Dong, K. Saitoh, and L. Dong, "Ytterbium-doped large-mode-area all-solid photonic bandgap fiber lasers" Opt. Exp. **22** (11), 13962-13968 (2014).
9. X. Ma, C. Zhu, I-Ning Hu, A. Kaplan, and A. Galvanauskas, "Single-mode chirally-coupled-core fibers with larger than 50μm diameter cores," Opt. Exp. **22** (8), 9206-9219 (2014).
10. J. M. Fini and J. W. Nicholson, "Bend compensated large-mode-area fibers: achieving robust single-modedness with transformation optics," Opt. Exp. **21** (16), 19173-19179 (2013).
11. D. Jain, C. Baskiotis, and J. K. Sahu, "Mode area scaling with Multi-trench rod-type fibers," Opt. Exp. **21** (2), 1448-1455 (2013).

12. D. Jain, C. Baskiotis, and J. K. Sahu, "Bending performance of large mode area muli-trench fibers," Opt. Exp. **21** (22), 26663-26670 (2013).
13. D. Jain, C. Baskiotis, T. C. May-Smith, J. Kim, and J. K. Sahu, "Large mode area multi-trench fiber with delocalization of higher order modes," [Invited], IEEE J. Sel. Top. Quantum Electron. **20**, 0902909-0902917 (2014).
14. D. Jain, Y. Jung, J. Kim, and J. K. Sahu, "Robust single-mode all-solid multi trench fiber with large effective mode area," Opt. Lett., **39** (17), 5200-5203 (2014).
15. D. Jain, C. Baskiotis, and J. K. Sahu, "Large mode area pixelated trench fiber," in *Speciality Optical Fiber, Advance photonics congress*, Barcelona, Spain, 2014, paper **SoW4B.3**.
16. S. R. Nagel, J. B. Macchesney, and K. L. Walker, "An Overview of the Modified Chemical Vapor Deposition (MCVD) Process and Performance," IEEE Transactions on Microwave Theory and Techniques **30** (4)**,** 305-322 (1982).
17. J. Stone, and C. A. Burrus, "Neodymium-doped silica lasers in end-pumped fiber geometry," App. Phys. Lett. **23** (7), 388-389 (1973).
18. J. E. Townsend, S. B. Poole, and D. N. Payne, "Solution-doping technique for fabrication of rare-earth-doped optical fibres," Electron. Lett. **23** (7), 329-331 (1987).
19. M.-J. Li, X. Chen, A. Liu, S. Gray, J. Wang, D. T. Walton, and L. A. Zenteno, "Limit of effective area for single-mode operation in step-index large mode area laser fibers," J. Lightwave Technol. **27** (15), 3010-3016 (2009).
20. V. Khitrov, J. D. Minelly, R. Tumminelli, V. Petit, and E. S. Pooler, "3kW single-mode direct diode-pumped fiber laser," in *Fiber Lasers XI, Photonic West conference*, San Francisco, Cali., 2014 Paper **8961.**
21. V. Matejec, I. Kasik, D. Berkova, M. Hayer, M. Chomat, Z. Berka, and A. Langrova, "Properties of optical fiber performs prepared by inner coating of substrate tubes," Ceramics Silikaty **45** (2), 62-69 (2001).
22. Y. H. Kim, U. C. Paek, and W. T. Han, "Effect of soaking temperature on concentrations of rare-earth ions in optical fiber core in solution doping process," Rare-earth doped Materials and Devices, V. Shibin Jiang, eds., Proc. SPIE **4282**, 123 (2001).
23. A. Dhar, M. C. Paul, M. Pal, A. K. Mondal, S. Sen, H. S. Maiti, and R. Sen, "Characterization of Porous core layer for controlling rare earth incorporation in optical fiber," Opt. Exp. **14** (20), 9006-9015 (2006).
24. D. Jain, Y. Jung, M. Nunez-Velazquez, and J. K. Sahu, "Extending single mode performance of all-solid large-mode-area single trench fiber," Opt. Exp. **22**(25), 31078-31091 (2014).
25. D. Jain, C. Baskiotis, J. Kim, and J. K. Sahu, "First demonstration of single trench fiber for delocalization of higher order modes," [Contributed upgraded to Invited] " in *Conference on Lasers and Electro-Optics* (CLEO), San Jose, Calif., 2014, paper SF1N.1.

1. Introduction

High power fiber lasers have revolutionized the laser world in the last decade [1]. Fiber lasers offer great advantages such as better power handling, good beam quality, and enhanced flexibility over solid-state lasers. Good beam quality and flexibility offered by optical fibers are also very attractive features for high power beam delivery. Conventional step index fiber (SIF), where core is doped with rare-earth ions has been used as a gain medium in fiber lasers and output power level in the range of kWs has been reported using these fibers [2]. However, non-linear effects often found to be the primary limiting factors for power scaling in fiber lasers and amplifiers [3]. Several fiber designs such as Photonic Crystal Fiber (PCF) [4], Leakage Channel Fiber (LCF) [5], Resonantly-enhanced Leakage Channel Fiber (Re-LCF) [6], Bragg fiber [7], 2D-All Solid Photonic Bandgap Fiber (2D-PBGF) [8], Polygonal Chirally Coupled Core (P-CCC) [9], bend compensated Parabolic Fiber [10], Multi trench Fiber (MTF) [11-14], and Pixelated Trench Fiber (PTF) [15] have been proposed to scale the effective area of the fundamental mode (FM) in order to increase the threshold of non-linear effects. However, most of these fiber designs such as PCF, LCF, Re-LCF, and 2D-ASPBGF are difficult to fabricate compared to SIF as they require stack and draw process due to their non-circular symmetry. Other designs offering cylindrical symmetry such as Bragg Fiber, bend

compensated parabolic fiber, and MTF are also complex to fabricate as compared to SIF, although relatively less challenging than non-circular symmetrical design. Moreover, core refractive index is required to be the same as that of the cladding in most of these designs such as PCF, LCF, Re-LCF, 2D-ASPBGF, Bragg fiber, MTF, and PTF and this requires micro-structuration or pixelation of doped core in order to match the refractive index with undoped cladding, which is a cumbersome process to do. On the other hand, SIF can be fabricated with conventional technique, such as Modified Chemical Vapor Deposition Process (MCVD) in conjunction with solution doping process [16-18] and suitable for mass production. Ming-Jun Li et al. demonstrated that the maximum scalable mode area for effective single mode operation from a SIF is 370μm^2 for 1060nm operation taking into account the core numerical aperture (NA) to be 0.06 that could be achieved experimentally at the time of publishing the paper in 2009 [19]. A single mode operation was ensured by bend-induced higher order modes (HOMs) loss to be higher than 10dB/m, while keeping the FM loss lower than 0.1dB/m at 1060nm.

However, our optimized solution doping process in conjunction with MCVD now shows the capability of controlling the NA as low as 0.038 with good reproducibility and good yield. This optimization has been achieved without the use of any pixelation and micro-structuring of the core. Moreover, achieved profile is flat along the cross-section of the core without any considerable dip. Recently, V. Khitrov et. al. has demonstrated a Yb doped SIF with NA of 0.048, although laser built with this fiber shows significant Raman generation at 3kW output power [20].

In this paper, we numerically showed the feasibility of achieving effective area around 700μm^2 from a SIF with a NA of 0.038, while following the same criterion of single mode operation (FM loss lower than 0.1dB/m and HOM loss higher than 10dB/m) at 1060nm wavelength. We then went on to fabricate a low NA (~0.038) 35μm diameter core Yb-doped SIF, using MCVD process in conjunction with solution doping technique. The qualitative analysis of the output beam of coiled fiber ensures a Gaussian beam despite different multi-mode beam excitation. Further, experimental characterizations ensure a good laser efficiency of 81% with M^2 less than 1.1.

2. Numerical simulations

Figure 1 shows the computed loss of the LP_{01} and LP_{11} (least lossy HOM) modes and effective area of the LP_{01} mode with respect to bend diameter for two different core sizes of a SIF at 1060nm, while core NA is fixed at 0.038 which corresponds to the refractive index difference (Δn) between core and cladding of 0.0005. Here we have considered the least lossy orientation of the LP_{11} mode which incidentally has the lowest loss as compared to other possible HOM. Losses were calculated using finite element method (FEM) based commercially available COMSOL software with additional circular anisotropic Perfectly Matched Layer (PML). Following the above mentioned criterion of loss (10dB/m for HOM and 0.1dB/m for FM), an effective area of 700μm^2 (taking bend induced distortion into account) can be achieved from a SIF having a core diameter of 35μm and at a bend diameter of 32cm. The loss ratio of FM to HOM remains above 130. However, core diameter larger than 35μm is unable to fulfil the above criterion as shown in Fig. 1. It is interesting to note that the bend diameter (32cm) achieved here is large as compared to the study performed by Ming-Jun Li et. al, in the case of 30μm core SIF for a fixed NA of 0.06, which is lower than 10cm and not ideal to inhibit bend induced mode deformation. An additional advantage offered by low NA SIF is that the issue of mechanical reliability of large diameter optical fiber under tight bending condition can be addressed too.

A bend diameter of 32cm is deemed to be large enough to avoid mechanical failure of the optical fiber, while it is small enough to maintain a compact device size. It is important to note that, the effective area achieved here is a significant improvement over the effective area (~370μm^2) offered by SIF with NA 0.06.

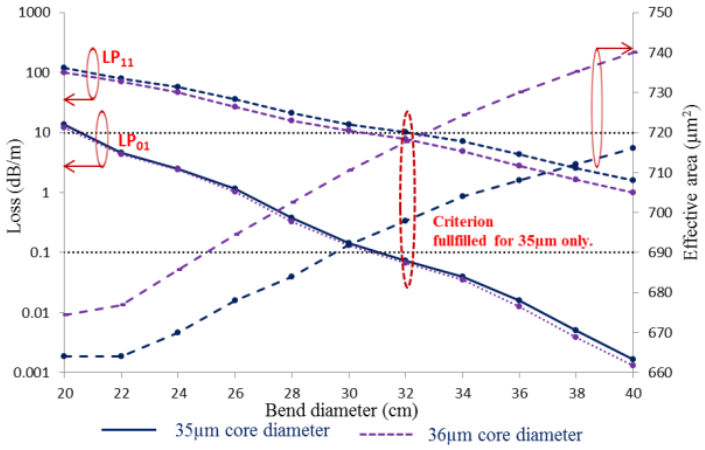

Fig. 1 The loss of LP_{01} and LP_{11} mode (least lossy orientation) and effective area of the LP_{01} mode of a SIF w.r.t. bending diameters at 1060nm for two different core diameters and with a fixed core Δn of 0.0005 (corresponding to an NA of 0.038). The loss of other HOMs is higher than LP_{11} modes.

3. Fabrication of ultra-low NA Yb-doped step index fiber

Rare-earth doped preforms are traditionally fabricated by MCVD process in conjunction with solution doping technique as follow: an un-sintered porous silica soot layer is deposited at reduced temperature after depositing the sintered cladding layers inside an ultra-pure silica tube. Soot layer is then soaked in a solution containing RE ions and co-dopants. Thereafter, solution is drained out of the tube and soot is dried. Dopants are then oxidized and soot layer is consolidated. Further, tube is collapsed to a solid rod. In this process, quantity of dopants (both rare-earth and co-dopants) incorporation decides the core refractive index as these are the only index raising components in silica soot. Therefore, in order to control the core refractive index it is necessary to control the dopants incorporation. Dopants incorporation depends on several aspects like soot porosity, solution doping condition, solution draining speed, and soot oxidation temperature etc for a particular solution strength [21-23]. However, soot porosity is the most important aspect as it not only decides the amount of the RE ion incorporation but also the uniformity of the profile. A non-uniform porosity can lead to a non-uniform profile especially a central dip, which can be detrimental to preserve singe mode operation. Moreover, uniformity of profile becomes very crucial when the required core refractive index is on the order of 10^{-4} to maintain effective single mode operation. It is pertinent to mention here that it is possible to control the soot porosity by controlling soot deposition temperature. In order to control the soot porosity, we performed several preform fabrications, using the same process parameters and solution strength but different soot deposition temperatures. We observed that soot deposition temperature plays a very crucial role in determining core refractive index with respect to cladding and over all profile of the core. After, optimizing the fabrication process, we fabricated a Yb doped SIF while achieving a very low Δn~0.0005. Figure 2 shows the refractive index profile of the fabricated preform at different distance along the length of the preform namely at 100mm, 200mm, and 300mm of a 350mm long preform. Figure 2 also shows the preform profile at two different angular positions i.e. 0 and 90 degrees represented by blue and red colors respectively. The measured preform profiles ensure good uniformity along the length of the preform. Moreover, refractive index profile maintains a flat profile along the cross-section, while maintaining a very low refractive index with respect to cladding. It is important to note that, we started with a 400mm long tube and ended up with ~350mm long usable preform ensuring a good yield of our

optimized process. The preform outer diameter is 12mm, while the diameter of the deposited core is 1mm.

The observed peaks at the center of the profiles are merely the measurement artifact. The surrounding regions of the core suffer from slight index perturbations caused by the deposited cladding layers. Outside this, the starting F300 tube constitutes the cladding. Typically refractive index of F300 tube is slightly larger than pure silica (e.g. ~0.00035 to 0.0005). In order to match the refractive indices of the deposited cladding and F300, a small quantity of Ge dopant is necessary. These index perturbations can be eliminated by avoiding cladding deposition altogether, so that F300 tube acts as a cladding region. We performed numerical simulations to study the impact of the small index perturbations and observed slight reduction of losses for both FM and HOM. For example, at 32cm bend diameter the loss of the FM is estimated to be ~0.07dB/m whereas for the LP_{11} mode it is ~9.23dB/m. These reductions are small compared to the ideal SIF and can be ignored.

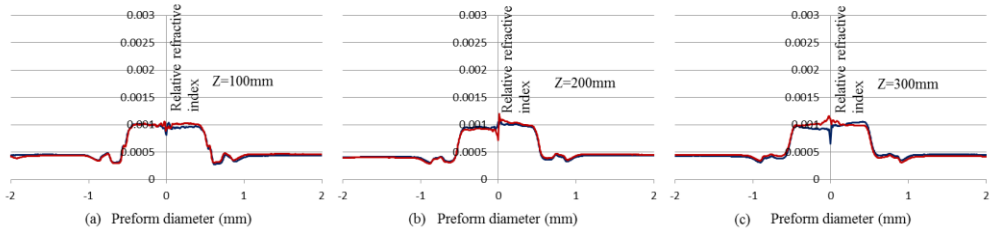

Fig. 2 The refractive index profile at different positions along the length of the preform. Blue and Red color corresponds to profiles at 0 degree and 90 degree angular positions respectively.

4. Characterization

The preform was first milled to a D-shape to facilitate the cladding pumping by breaking the circular symmetry and subsequently drawn in to a fiber with an outer diameter of 420µm so as to have a 35µm core diameter. Fiber was coated with a low index polymer to allow pump light to be guided in the cladding. Figure 3(a) shows the CCD image of the cladding geometry of the fiber by launching a 1060nm laser into the cladding. The output profile shows cladding modes and a D-shape outer cladding. Figure 3(b) shows the white light transmission spectra for both unbent and bent conditions of a 1.26m long fiber. The absorption at ~975nm is 2dB/m for both straight and bent fibers.

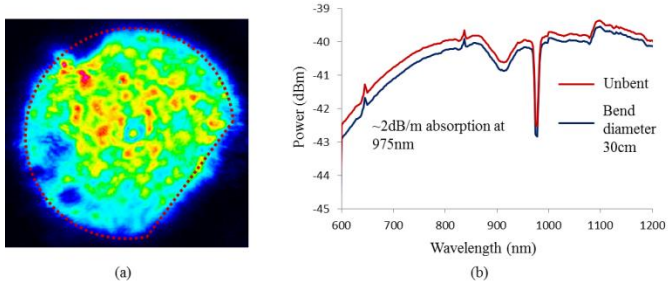

Fig. 3 (a) Output image of the fiber at 1064nm captured with a CCD camera. (b) White light transmission spectra of 1.26m long fiber in bend and unbent configurations.

In order to verify the effective single mode behavior, we investigated the output beam profile for different lengths and bend diameters of the fiber. Figure 4 (a) shows the experimental set-up used for the investigations. A 1060nm laser beam is coupled into the core using two lenses namely collimating and focusing lens. We have also used a binary phase plate to change the

mode profile of the input beam, while a CCD camera is used to analyze the output beam profile. We removed the low-index coating at both ends of the fiber under test and applied index-matching oil to strip-off the cladding modes. First, we used a 1.55m long fiber in a straight condition with a slight bend as shown in the experimental set-up. A slight bend was required as we did not have enough space on our optical table. Figure 4(c) shows the output beam profile with respect to LP_{01} mode of launch beam. Here LP_{01} mode was the direct output from a single-mode laser source delivered by a conventional single mode fiber as shown in Fig. 4(a). Output beam profile (as shown in Fig. 4(c)) is clearly non-Gaussian and shows significant presence of the HOMs. Moreover, fiber output as shown in Fig. 4(d) clearly shows the LP_{11} mode when a mixed mode (LP_{01} +LP_{11}) as shown in Fig. 4(b) was launched using binary phase plate. This ensures poor suppression of the HOMs and this is in good agreement with our simulation study, which also indicated a multi-mode behavior under unbent condition.

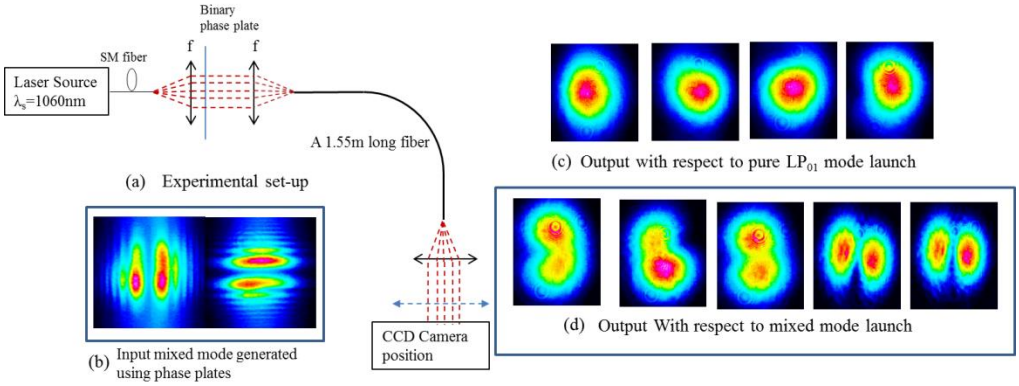

Fig. 4 (a) Experimental set-up for modal verification of the fiber, (b) input mixed modes (LP_{01} and LP_{11}) using phase plate, (c) output beam profiles for LP_{01} mode launch, and (d) output beam profiles for a mixed mode launch.

Afterwards, we bent the fiber to a diameter of ~32cm (+/- 0.5cm) as shown in Fig. 5(a) keeping rest of the experimental conditions same. We observed dramatic improvement in the output beam profile. The output beam appears to be a near Gaussian profile as shown in Fig. 5(b) due to the bend induced loss of the HOMs. We also measured the output power levels, when LP_{01} and mixed modes were independently launched into the fiber for different bend diameters as shown in Fig. 5(c). This is a clear evident of a significant discrimination between LP_{01} and LP_{11} modes under bending. In order to improve the quality of the output beam profile, we increased the length of the fiber under test to ~3m to increase the aggregate loss for all the HOMs. The profile of the output beam becomes almost Gaussian for the same bend diameter of ~32cm (+/- 0.5cm). We also launched multimode beam (dominating LP_{11} content as shown in the left hand column of Fig. 6(c)) into the fiber, however the output beam maintains Gaussian profile as shown by the right hand columns in Fig. 6(c). These measurements verify that an effective single mode operation can be obtained from a low NA (~0.038) SIF by choosing an appropriate bend diameter.

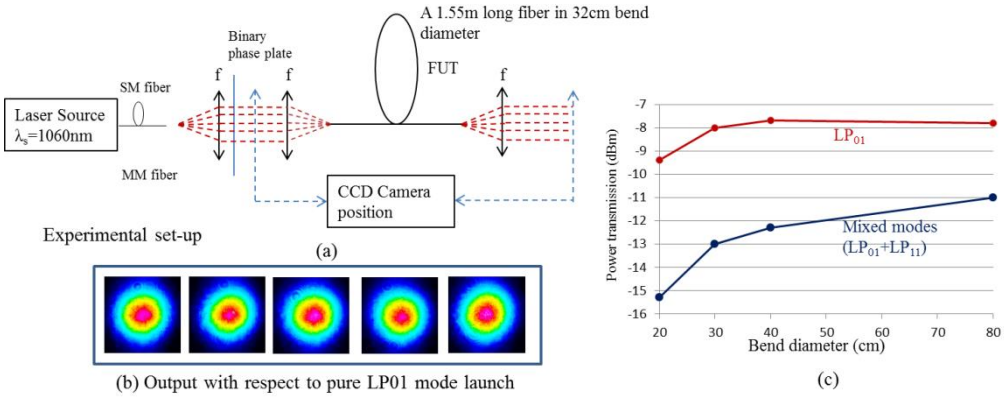

Fig. 5 (a) Experimental set-up for single mode verification, (b) Output beam with respect to LP_{01} mode launch, and (c) output power with respect to LP_{01} and LP_{11} modes launch at different bend diameters. A 1.55m long fiber coiled at ~32cm (+/- 0.5cm) bend diameter was used in this experiment.

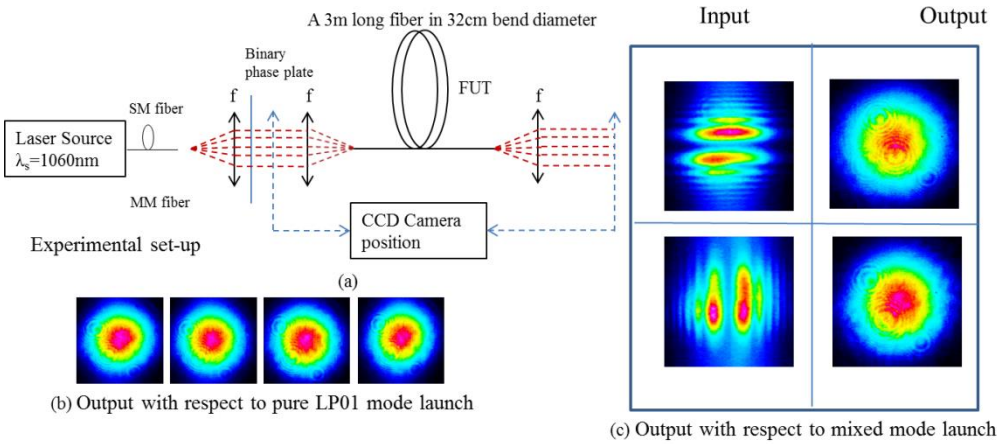

Fig. 6 (a) Experimental set-up for single mode verification, (b) profile of the output beam with respect to LP_{01} mode launch, and (c) profile of output beam with respect to mixed mode launch. A 3m long fiber coiled at ~32cm (+/- 0.5cm) bend diameter was used in this experiment.

5. Laser efficiency measurement

We measured the fiber laser efficiency in a 4%-4% laser cavity using a 7m long fiber as shown in Fig. 7(a). A multimode diode laser operating at ~975nm was used as a pump source. Fiber under test was kept with a bend diameter of ~32cm (+/- 0.5cm). Figure 7(b) shows the measured slope efficiency with respect to absorbed pump power. A maximum output power of 50W was obtained at a launched pump power of ~72W that corresponds to a slope efficiency of ~81% with respect to absorbed pump power. Further power scaling was limited by the available pump power. Inset shows the output beam profile with a measured M^2 of ~1.07 in the x-direction and 1.09 in the y-direction. The spectral profile of the free running laser is shown in Fig. 7(c) with the multiple peaks located at ~1040nm.

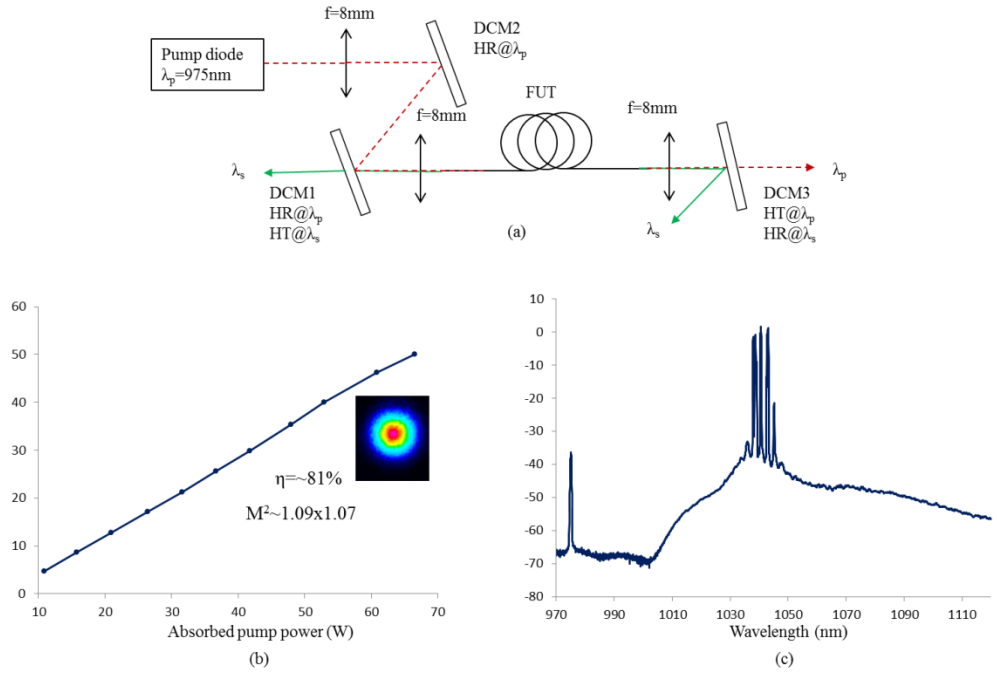

Fig. 7 (a) Experimental set-up used for laser efficiency measurement, DCM-Dichroic mirror, FUT-fiber under test, HR-High reflectivity, HT-High transmission, λ_p=pump wavelength, and λ_s=signal wavelength, (b) output power as a function of pump power of 4%-4% laser cavity. Inset shows the output beam profile, and (c) output spectrum taken with an OSA (ANDO (AQ6370B)) resolution of 0.2nm.

6. Discussion

Our optimized MCVD process and solution doping technique has shown the versatility to realize ultra-low NA rare-earth doped fibers. It is important to note that PCFs were seen as a potential candidate for fiber lasers for large effective area because of their capability to achieve lower NA than SIF due to presence of air holes in their cladding. However, our current state of the art fabrication process to achieve an ultra-low NA brings SIF in a closer competition to PCF for mode area scaling. In the last decade, there have been several demonstrations of large mode area fibers of various kinds such as PCF based designs like LCF and Re-LCF, photonic band gap based designs like 2D-ASPBF and Bragg fiber, different versions of SIF like parabolic fiber and W-type fiber, and resonant coupling based designs like MTF, PTF, and P-CCC claiming better mode area scaling capability than SIF. However, it is important to compare the achievable effective area of the FM not the core size offering similar level of suppression of the HOMs (e.g. 10dB/m) and low loss for the FM mode (e.g. 0.1dB/m) in a reasonable device size (for which the bend diameter is considered to be lower than 40cm) to find out any additional advantages offered by these designs.

Our analysis concludes that some of these designs have the capability of achieving effective area as large as 1000μm^2 at 1060nm following above mentioned criterion of effective single mode operation (FM loss lower than 0.1dB/m and HOM loss higher than 10dB/m) for a compact size device (bend radius with in 40cm) thanks to the pertinent efforts of the researchers across the globe [24]. However, this increment comes at the cost of associated difficulties in fabrication process. There are also additional drawbacks like cleaving

and splicing in the case of PCF due to presence of air hole and reduced pump cladding efficiency in case of 2D-ASPBGF due to the presence of high index elements in the cladding. Beyond any doubt, SIF is the simplest design to implement and not known to suffer from any additional difficulties. Prior to this demonstration, a low-NA of 0.048 was reported for Yb-doped SIF [20]. Table 1 shows the comparative analysis of mode area scaling capability of SIF with different NAs.

Table 1 comparative analysis of mode scaling for different NA.

NA (corresponding to Δn)	**Maximum effective area in μm^2 (0.1dB/m for FM and 10dB/m for HOMs), taking bend induced distortion into account**	**Required bend diameter in cm (for 10dB/m loss for the HOMs and less than 0.1dB/m for FM)**	**Core diameter (μm)**
0.048 (0.0008)	~450	~15.5	~29
0.038 (0.0005)	~700	~32	~35

It is evident from Table 1 that for 0.048 NA, maximum scalable mode area is ~450μm^2 for a ~29μm core at a bend diameter of ~15.5cm. On other hand in case for 0.038 NA the maximum scalable mode area is ~700μm^2 for a ~35μm core and at a bend diameter of ~32cm. This is a significant improvement in terms of mode area scaling for SIFs. We believe that after this study, fiber laser manufactures will have a reason to look back to SIF for mode area scaling.

Moreover, we recently proposed a Single-trench fiber (STF), which needs an additional high index ring surrounding the core of ultra-low NA SIF [24-25]. Our studies show that addition of ring significantly enhances the suppression of HOMs by delocalizing the HOMs [24-25]. Our detailed studies ensure that the effective area larger than 1,000μm^2, while offering HOMs losses to be larger than 10dB/m and FM loss to be lower than 0.1dB/m and a more than 30% difference in power fraction of FM and HOMs in core region can be achieved at 20cm bend radius and at 1060nm wavelength [24-25]. STF offers a number of advantages over other competitive fiber designs. We believe that after SIF, STF is the easiest fiber design to realize for fiber laser applications. The mode area scaling of both SIF and STF has come true only by the realization of ultra-low NA (0.038) core thanks to our optimized MCVD and solution doping process.

7. Conclusion

We have successfully demonstrated an Yb-doped SIF with the core having a flat refractive index profile and an ultra-low-NA of 0.038. The fiber is fabricated using the state of the art MCVD and solution doping technology. Numerical simulations ensure an effective area of 700μm^2 from a 35μm core fiber at 32cm bend diameter. This is a significant improvement as compared to the effective area obtained with core NA of 0.048 in previous study. Our detailed characterization ensures an effective single-mode operation at 1060nm at a bend diameter of ~32cm (+/- 0.5cm). Furthermore, when tested in a laser configuration the fiber shows a ~81% slope efficiency with beam quality factor M^2 of less than 1.1 indicating an effective single mode operation.

Acknowledgement

The work is supported by the EPSRC Centre for the Innovative manufacturing in Photonics EP/HO2607X/1.